$HfSe_2$ Thin Films: 2D Transition Metal Dichalcogenides Grown by Molecular Beam Epitaxy

Ruoyu Yue,[†,§] Adam T. Barton,[†,§] Hui Zhu,[†] Angelica Azcatl,[†] Luis F. Pena,[†] Jian Wang,[†] Xin Peng,[†] Ning Lu,[†] Lanxia Cheng,[†] Rafik Addou,[†] Stephen McDonnell,[†] Luigi Colombo,[‡] Julia W. P. Hsu,[†] Jiyoung Kim,[†] Moon J. Kim,[†] Robert M. Wallace,[†] and Christopher L. Hinkle*[,†]

[†]Department of Materials Science and Engineering, University of Texas at Dallas, Richardson, Texas 75080, United States and [‡]Texas Instruments, Dallas, Texas 75243, United States. [§]R. Yue and A. T. Barton have contributed equally to this work.

ABSTRACT In this work, we demonstrate the growth of $HfSe_2$ thin films using molecular beam epitaxy. The relaxed growth criteria have allowed us to demonstrate layered, crystalline growth without misfit dislocations on other 2D substrates such as highly ordered pyrolytic graphite and MoS_2. The $HfSe_2$ thin films exhibit an atomically sharp interface with the substrates used, followed by flat, 2D layers with octahedral (1T) coordination. The resulting $HfSe_2$ is slightly n-type with an indirect band gap of ~1.1 eV and a measured energy band alignment significantly different from recent DFT calculations. These results demonstrate the feasibility and significant potential of fabricating 2D material based heterostructures with tunable band alignments for a variety of nanoelectronic and optoelectronic applications.

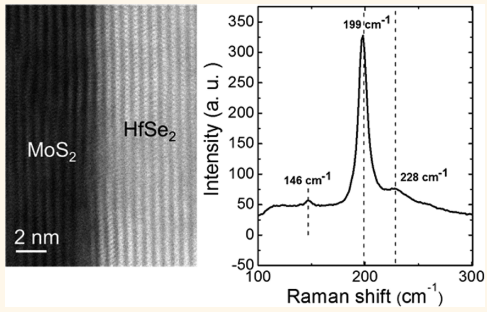

KEYWORDS: hafnium diselenide · van der Waals epitaxy · heterostructure · transition metal dichalcogenides · tunnel field-effect transistors

The continued need for high-speed and low-power electronics beyond the current silicon-based devices has prompted the recent exploration of new materials such as graphene that have unique physical and electronic properties.[1,2] However, the intrinsic lack of a band gap in graphene has redirected interest to other two-dimensional (2D) materials that have a band gap such as transition metal dichalcogenides (TMDs) of the form MX_2, where M is a transition metal from group IVB (Ti, Zr, Hf) or group VIB (Mo, W) and X is a chalcogen (S, Se, or Te).[3,4]

TMDs are layered materials and are stacked in the form of X−M−X sandwiches with a plane of metal atoms in the middle of two hexagonal planes of chalcogen atoms.[5,6] As 2D materials, the adjacent layers are held together by weak van der Waals interactions and, in principle, without surface dangling bonds.[7] The electronic structure (band gap and electron affinity for example) can be tailored through the strategic selection of the transition metal and chalcogen.[8] Additionally, the band gap can be "tuned" as a function of the number of X−M−X layers due to quantum confinement.[9−11] For instance, the MoS_2 bulk indirect band gap of 1.23 eV[12] increases to a direct band gap of 1.8 eV for a single layer of MoS_2.[13] This suggests significant flexibility in creating promising heterostructures with useful electronic properties with varying band offsets.

The heteroepitaxial growth of TMDs via van der Waals epitaxy (VDWE) was first introduced by Atsushi Koma in 1984 by demonstrating molecular beam epitaxy (MBE) growth of layered $NbSe_2$ on 2H MoS_2.[14] Following $NbSe_2$ growth, distinct changes in the reflection high energy electron diffraction (RHEED) pattern and low-energy electron-loss spectroscopy (LEELS) spectra indicated that smooth, crystalline, unstrained $NbSe_2$ with subnanometer thickness could be grown on MoS_2 despite the 10% lattice mismatch. Due to the very low density of dangling bonds and weak interaction between interfaces, these layered 2D materials have a relaxed lattice matching

* Address correspondence to chris.hinkle@utdallas.edu.

Received for review October 3, 2014 and accepted December 11, 2014.

Published online December 11, 2014
10.1021/nn5056496

condition.[15−19] 2D heterostructures have previously been shown to be of relatively high crystalline quality even when grown on a substrate with 58% lattice mismatch.[20]

Among all of the TMD materials, very few studies have been performed on HfX_2 (X = S, Se, Te) compounds.[21−23] The Hf-based TMDs are predicted to be small-gap semiconductors with large work functions and reasonable mobilities, making them suitable for a range of nanoelectronic and optoelectronic device applications. For example, recent first-principles calculations suggest that $HfSe_2$ can be used as the drain in vertically stacked, "broken-gap" band alignment tunnel field-effect transistors (TFETs) primarily due to the predicted high electron affinity of the Hf-based TMDs compared to other prevailing TMDs.[8] Although there are a few experimental reports on the electrical and optical properties of bulk HfX_2 materials, the previous work focused on bulk materials grown by chemical vapor transport, a method that is not well suited for the growth of precise and uniformly thick films needed to investigate the layer-dependent properties of TMDs and take advantage of the properties of layered thin films.[24,25] In this work, we demonstrate for the first time the growth of $HfSe_2$ thin films using molecular beam epitaxy. This $HfSe_2$ growth on other 2D materials reveals the unique opportunities for fabricating all 2D heterostructures with appropriate band alignments to be utilized in novel nanoelectronic and optoelectronic devices.[4,8,26,27]

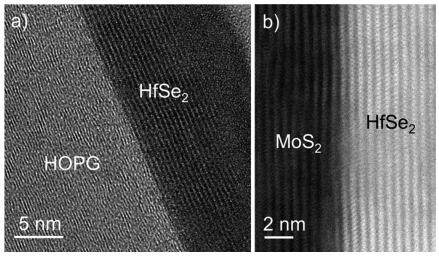

Figure 1. (a) TEM image of grown $HfSe_2$ on HOPG and (b) HADDF-STEM image of grown $HfSe_2$ on MoS_2 showing abrupt interfaces and layered crystalline films.

RESULTS AND DISCUSSION

Structural Characterization. Figure 1 shows the cross-sectional transmission electron microscopy (TEM) image of the MBE grown $HfSe_2$ (∼15 nm thick) on highly ordered pyrolytic graphite (HOPG) and high angle annular dark field (HAADF)-scanning transmission electron microscopy (STEM) image of MBE-grown $HfSe_2$ on MoS_2 achieved in this current investigation. It can be observed that the layered films have atomically abrupt interfaces with each substrate and are uniform. This demonstrates that it is possible to have layered growth of $HfSe_2$ using van der Waals epitaxy without misfit dislocations associated with a lattice mismatch as large as 41%. The interlayer distance of the layered $HfSe_2$ is measured to be ∼0.62 nm, consistent with the reported value of 0.614 nm for bulk $HfSe_2$ crystals.[21] The scanning tunneling microscopy (STM) images of the same $HfSe_2$ on HOPG are shown in Figure 2, where the hexagonal top surface structure of $HfSe_2$ is revealed, while scanning tunneling spectroscopy (STS) measurements show a band gap of ∼1.1 eV with a Fermi level above midgap (slightly n-type). Optical absorption results obtained in this work and by others previously reported in the literature[21,22] are consistent with an indirect band gap of this value. The STM image in Figure 2b shows the nucleation of a new layer on top of the existing 15 nm thick $HfSe_2$ film. The grain size of the underlying $HfSe_2$ layers is in general greater than 100 nm × 100 nm, and the $HfSe_2$ step edge height is about 0.6 nm, consistent with the height of one monolayer of $HfSe_2$. Increasing the grain size and understanding the nucleation mechanism of $HfSe_2$ crystal growth is the focus of ongoing research. Out-of-plane X-ray diffraction (XRD) data of this same $HfSe_2$ on HOPG reveals a strong (001) peak at 14.2° and the (003) peak at 43.8°,[28] consistent with calculations assuming an unstrained 1T $HfSe_2$ crystal structure.

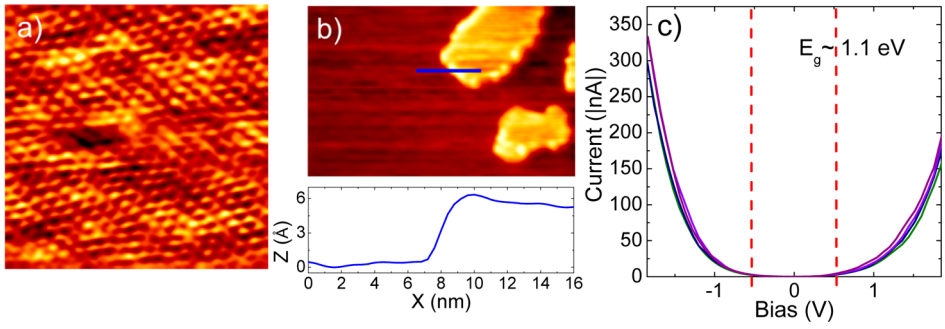

Figure 2. STM of ∼15 nm grown $HfSe_2$ on HOPG showing (a) atomic resolution with hexagonal surface symmetry (image conditions were 5 nm × 5 nm, V_{bias} = 0.2 V, I_t = 0.5 nA) and (b) an additional layer beginning to form on top of a large-area previous layer with a 0.6 nm step height (50 nm × 50 nm, V_{bias} = 2 V, I_t = 0.2 nA). (c) STS $|I|-V$ curves show a measured band gap of ∼1.1 eV, consistent with absorption data. E_F is slightly above midgap. The multiple curves shown are STS measurements at different points on the $HfSe_2$. Each of the curves is an average of 10 measurements at that point. This was done to show the repeatability and uniformity of the measurements and film.

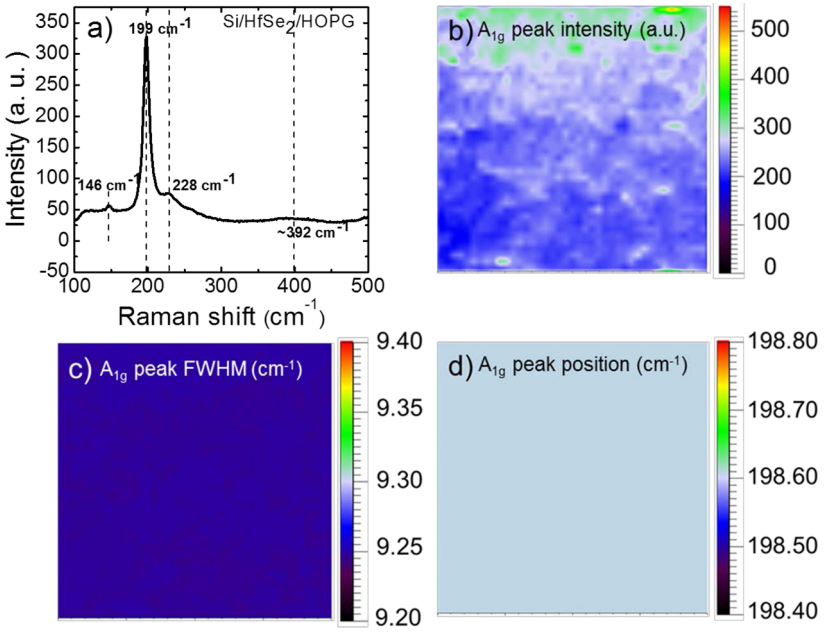

Figure 3. (a) Raman spectroscopy of Si-capped $HfSe_2$ grown on HOPG and corresponding Raman map of the 199 cm^{-1} peak (b) intensity, (c) full width at half-maximum (fwhm), and (d) position over a 20 μm × 20 μm area showing uniform growth quality over a large area. The gradient of peak intensity in part b is due to vibrations of the Raman table (caused by building vibrations), causing the sample to drift slightly out of focus during the measurements and not due to a change in film quality/thickness.

Raman data plotted in Figure 3 show that the E_g and A_{1g} are the Raman-active modes[29,30] at 146 and 199 cm^{-1}, respectively. Raman mapping of the A_{1g} peak over a 20 μm by 20 μm area shows full coverage and excellent uniformity in crystal quality over this large area. The Raman results are in agreement with previous reports of bulk $HfSe_2$ grown by iodine-vapor phase transport as well as the calculated mode frequencies of the octahedral 1T structure of $HfSe_2$.[30,31] These Raman peak positions in conjunction with the XRD data and the RHEED analysis discussed later all indicate that the grown $HfSe_2$ is unstrained, one of the hallmarks of van der Waals epitaxy as performed here. The grown material and the substrate interact only through weak van der Waals interactions, which is quite different than the typical covalent interactions observed in normal heteroepitaxy. The impact of lattice mismatch is very small despite the large values of mismatch and does not introduce measurable strain into the films. This is consistent with the early VDWE findings by the Koma group.[14] Calculations based on thermodynamic stabilities predict the 1T phase to be the preferred $HfSe_2$ polytype,[8] consistent with all of the experimental results in this study.

Experimentally Determined Band Alignment. The band gap measured by STS (~1.1 eV), as mentioned above, while consistent with the 1.13 eV experimentally measured band gap values of bulk $HfSe_2$ grown by iodine-vapor phase transport,[21,22] is quite different from that predicted by density function theory (DFT) calculations of about 0.5 eV. To further investigate the electronic structure of our grown $HfSe_2$, a series of measurements were employed (Figure 4). The work function of the $HfSe_2$ grown on HOPG, measured by the X-ray photoelectron spectroscopy (XPS) low-energy cutoff and by Kelvin probe measurements in air, is ~4.4 eV in ultrahigh vacuum (UHV) and ~3.83 eV in air, both significantly lower than the DFT-calculated work function value of 5.9 eV. The valence band edge, as measured by XPS, was determined to be ~0.7 eV below the Fermi level, *i.e.*, 5.1 eV away from the vacuum level in UHV, and the ionization potential as determined by the threshold of photoelectron yield in photoelectron spectroscopy in air (PESA)[32] is ~4.93 eV; again both values are significantly lower than the DFT prediction of 6.2 eV. This experimental determination of the band alignment, confirmed by multiple characterization techniques, is consistent with the same measurements performed on bulk $HfSe_2$ crystals grown by chemical vapor transport (CVT)[28] as well as other published band alignment data of hafnium disulfide (HfS_2) films.[21,23] The discrepancies between our experimentally determined band alignment and the previously reported DFT calculations stem from (1) the common underestimation of band gaps in DFT, (2) a transcription error in ref 8, which reported larger work functions than are calculated, and (3) surface species that modify the experimentally measured work function with respect to the DFT-calculated ideal surfaces. These surface species will now be discussed.

$HfSe_2$ Chemical Analysis and Surface Oxidation Reactivity. The XPS spectra of $HfSe_2$ grown on HOPG at a substrate temperature of 550 °C are shown in Figure 5. The Hf 4f spectrum in Figure 5a is composed of two chemical states, $HfSe_2$ and HfO_x. We also detect two chemical

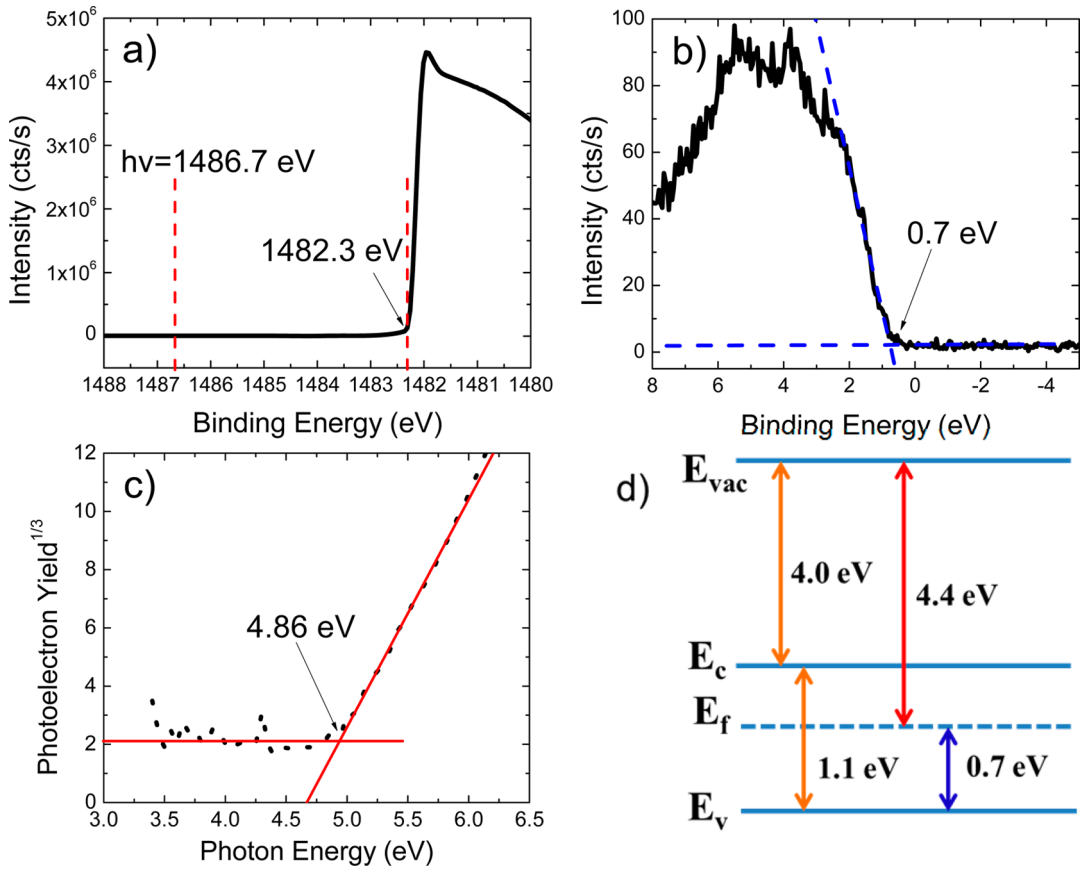

Figure 4. (a) XPS low-energy cutoff shows a measured work function of ~4.4 eV for $HfSe_2$ grown on HOPG; (b) XPS valence band edge shows E_V resides 0.7 eV below the E_F, suggesting n-type behavior consistent with STS; (c) ionization potential measured as the threshold of photoelectron yield in photoelectron spectroscopy measurements of $HfSe_2$/HOPG in air; (d) proposed energy band alignment of $HfSe_2$ from experimental measurements. This differs significantly from recent DFT calculations.

states in the Se 3d spectrum shown in Figure 5b, assigned to Se−Hf bonding ($HfSe_2$) and a Se−Se chemical state. Curve fitting and calculations show that the Hf:Se ratio in the crystalline $HfSe_2$ is 1:1.96, which is ~1:2 within the experimental error of XPS atomic sensitivity factors.[33] It should be noted that slight deviations in stoichiometry (slightly Se deficient for example) should not strongly impact the band alignment. Recent DFT calculations[34] have shown that chalcogen vacancies do not affect the energetic alignment of the conduction or valence bands, nor do they act as dopant levels. Therefore, we do not believe that deviation from stoichiometric $HfSe_2$ is the reason for the differences between the DFT and experimental band alignment.

The HfO_x state seen in Figure 5 is caused by exposure to air postgrowth and not oxygen in the layered $HfSe_2$, which was confirmed by electron energy loss spectroscopy (EELS) analysis of samples that were capped *in situ* with a-Si.[28] To further investigate the $HfSe_2$ top layer oxidation, a temperature study of $HfSe_2$ grown on HOPG with substrate temperatures ranging from 400 to 550 °C was performed with all other parameters held constant. It can be clearly observed in Figure 5c that when the substrate temperature is increased from 400 to 550 °C, the Hf-oxide that grows upon air exposure is decreased significantly, indicating that the higher growth temperature results in a more chemically stable $HfSe_2$ film that has improved crystalline quality and is more resistant to top surface oxidation. Similar oxidation of the $HfSe_2$ top surface was also seen in purchased $HfSe_2$ bulk crystals grown by CVT at $T > 900$ °C.[35] The Hf 4f spectrum acquired from a CVT-grown sample exfoliated using Scotch tape and exposed to air for 5 min shows approximately the same level of top surface oxidation as our MBE-grown samples, while *in situ* exfoliation of the purchased samples reveals no detectable oxygen in the film.[28] The oxidation of all TMDs is calculated to be thermodynamically favorable (in contrast to graphene). However, the oxygen adsorption kinetics are quite different for the disulfides compared to the diselenides and lead to the differences in surface oxidation between MoS_2 and $HfSe_2$, for example. The hybridized M−X d-band center lies deeper for the sulfides compared to the selenides, indicating stronger bonding in the sulfides. This leads to a higher oxygen adsorption kinetic barrier and less oxidation of the sulfides for a given time.[36]

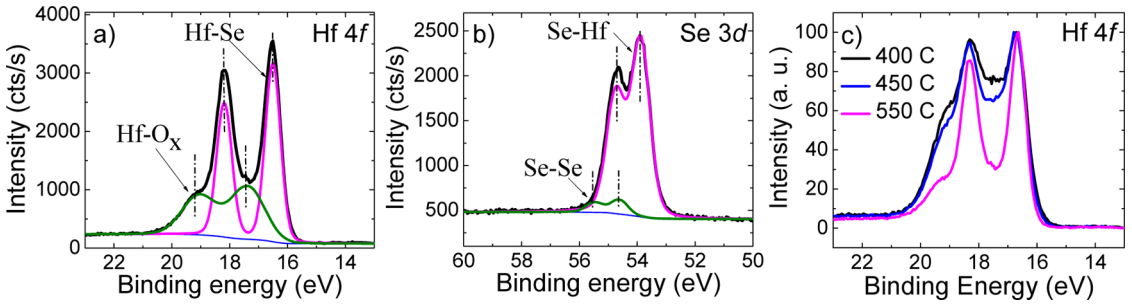

Figure 5. (a) XPS spectra showing a narrow, sharp crystalline $HfSe_2$ chemical state and HfO_x caused by air exposure postgrowth; (b) XPS spectra of Se 3d for $HfSe_2$ on HOPG; (c) XPS of $HfSe_2$ grown at different substrate temperatures: the higher the growth temperature, the less oxidation upon air exposure.

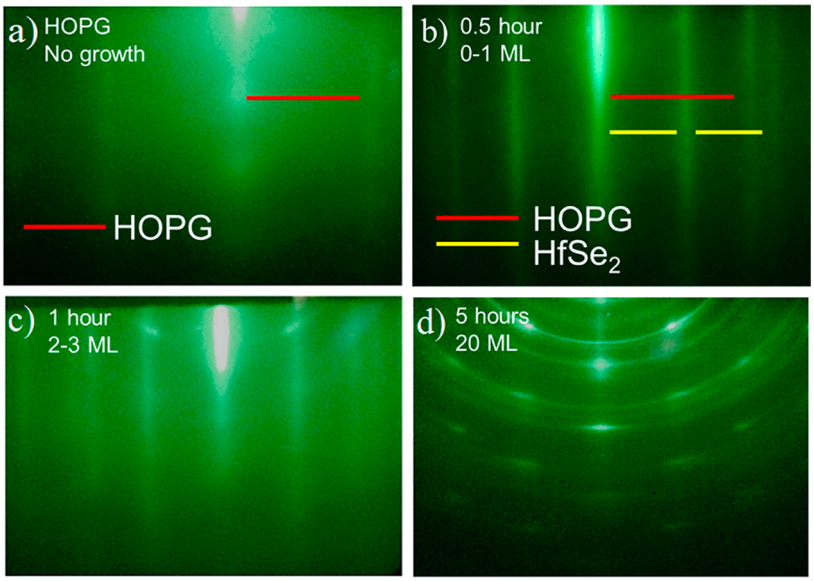

Figure 6. RHEED progression during the growth of $HfSe_2$ on HOPG. (a) HOPG with no $HfSe_2$ growth; (b) 0.5 h $HfSe_2$ growth (0−1 ML) shows two sets of streaks corresponding to the reciprocal lattices of HOPG and $HfSe_2$; (c) 1 h growth (2−3 ML) shows faint broken Debye rings indicating the onset of islanding; (d) 5 h growth (20 ML) shows full Debye rings with underlying streaks.

Additionally, the transition metal also plays an important role in the surface oxidation, as initial experiments show that HfS_2 films oxidize more easily than MoS_2 films.[28]

RHEED Progression to Determine Growth Mode. *In situ* RHEED patterns were measured to understand the growth process of $HfSe_2$ on HOPG at 450 °C. Before the growth of $HfSe_2$, long streaks were observed as shown in Figure 6a; these are indicative of a flat, crystalline top surface of HOPG. After 0.5 h growth (0−1 ML), an additional set of streaks appeared (Figure 6b). The ratio of the line spacing in the RHEED pattern matches the ratio of lattice constants of $HfSe_2$ and HOPG. This suggests that the initial growth of $HfSe_2$ is not pseudomorphic and is unstrained, as the $HfSe_2$ has its own lattice structure rather than taking on the substrate's lattice. Initial characterization of the grown thin TMD film indicates that the layers are rotationally aligned with the underlying substrate, consistent with a previous VDWE TMD growth reported in the literature.[16]

After 1 h of deposition (2−3 ML), Debye rings begin to appear (Figure 6c), suggesting the onset of islands and polycrystalline film formation. Following 5 h of growth (20 ML), the RHEED patterns (Figure 6d) are composed of complete Debye rings with underlying streaks. This progression indicates that the initial growth occurs in a 2D growth mode with rotational alignment to the substrate but with its own lattice structure. However, as the growth proceeds, nucleation-driven islanding occurs. We anticipate that the onset of islanding can be delayed and the domain size can be increased through the reduction of the nucleation frequency by reducing the Hf flux as previously reported for $NbSe_2$ growth.[37]

CONCLUSIONS

In summary, we have demonstrated the growth of 2D, crystalline $HfSe_2$ thin films by molecular beam epitaxy. The advantages provided by the van der Waals epitaxy growth method has allowed for layered,

crystalline growth on HOPG and MoS_2 substrates with no detectable misfit dislocations or strain in the films despite lattice mismatches of 41% and 17%, respectively. The $HfSe_2$ thin films exhibit an atomically sharp interface with the substrates used, followed by flat, 2D layers with octahedral (1T) coordination. The resulting $HfSe_2$ is slightly n-type with a band gap of ~1.1 eV and a measured energy band alignment significantly different from recent DFT calculations. The demonstration of $HfSe_2$ growth on other 2D materials demonstrates the unique opportunities for fabricating all 2D heterostructures with appropriate band alignments to be utilized in novel nanoelectronic and optoelectronic devices.

MATERIALS AND METHODS

HOPG and MoS_2 substrates were purchased from SPI Supplies.[38] $HfSe_2$ grown by chemical vapor transport was purchased from 2D Semiconductors.[35] $HfSe_2$ growth was performed in a VG-Semicon V80H molecular beam epitaxy system that is part of a three-chamber MBE cluster system with each of the growth chambers interconnected with UHV transfer tubes (base pressure = 10^{-11} mbar). The TMD growth chamber is equipped with a vertical e-beam evaporator enabling the growth of high melting temperature metals such as Hf, Ti, Mo, and W in addition to effusion cell evaporation of the chalogens. Each growth chamber is equipped with *in situ* RHEED. $HfSe_2$ thin films were grown on ~1 × 1 cm^2 mechanically exfoliated HOPG and MoS_2. The substrates are held at 450 °C for 2 h in the growth chamber prior to growth to complete the atomically clean surface preparation. Before each growth, the Hf and Se sources were outgassed for 2 h. During the growth, the pressure was maintained at ~1×10^{-9} mbar and the substrate temperature was kept at 450 °C except when specifically mentioned. The Se:Hf flux was maintained at a 5:1 ratio. The Se and Hf shutters were opened and closed simultaneously, and the growth rate was determined to be 0.05 nm/min. For several experiments, an *in situ* deposition of amorphous Si was used as a capping layer to eliminate the effects of atmospheric exposure on the top surface of the $HfSe_2$.

XPS was carried out *ex situ* using a monochromated Al Kα source ($h\upsilon$ = 1486.7 eV) and an Omicron EA125 hemispherical analyzer. The analyzer acceptance angle of 8°, takeoff angle of 45°, and pass energy of 15 eV were employed in this study. Spectra were deconvolved using the curve-fitting software AAnalyzer,[39] and the stoichiometry of the $HfSe_2$ was determined using relative sensitivity factors for the Hf 4f and Se 3d core levels of 2.05 and 0.67, respectively.[33] The features were fit with Voigt line shapes with an active Shirley background subtraction.[40]

The surface structure of the $HfSe_2$ was examined in a separate UHV chamber (base pressure ~2×10^{-11} mbar) using an Omicron variable-temperature scanning tunneling microscope.[41] All the STM images were obtained under constant current mode at room temperature, without any thermal treatment prior to imaging. The images were processed using WSxM software.[42] The $I-V$ spectra were obtained from an average of 10 curves.

Raman spectra acquisition was performed with a Renishaw confocal Raman system. The laser excitation wavelength is 532 nm. A 1% Raman laser power, corresponding to 0.229 mW, and 0.4 nm scanning step were used in the Raman mapping characterization.

The ionization potential was measured by photoelectron spectroscopy in air (AC2, RKI instrument) at an excitation power of 100 nW. The work function was measured in air (in the dark) using a Kelvin probe (KP Technology) with a stainless steel tip (2 mm diameter, ~4.2 eV work function). Before sample measurements, the tip work function is calibrated against a piece of 100 nm thick gold sample. The work function of the gold sample stored in air is ~5.1 eV,[43] which is also confirmed by photoelectron spectroscopy in air.

A Rigaku Ultima III X-ray diffractometer system was employed for $HfSe_2$ thin-film diffraction characterization. Data were acquired in a symmetric geometry ($2\theta-\theta$ scan) using parallel beam optics. TEM cross-sectional samples were made by FIB-SEM Nova 200 with a lift-out method. A JEM-ARM200F transmission electron microscope operated at 200 kV with probe aberration corrector was used for $HfSe_2$ cross-section imaging and EELS analysis.

Conflict of Interest: The authors declare no competing financial interest.

Acknowledgment. The authors acknowledge useful discussions with Prof. K. J. Cho. This work is supported in part by the SWAN Center, a SRC center sponsored by the Nanoelectronics Research Initiative and NIST. It is also supported in part by the Center for Low Energy Systems Technology (LEAST), one of six centers of STARnet, a Semiconductor Research Corporation program sponsored by MARCO and DARPA. This work is also supported in part by the Texas Higher Education Coordinating Board's Norman Hackerman Advanced Research Program. J.W. is supported by National Science Foundation (DMR-1305893), and J.W.P.H. acknowledges the Texas Instruments Distinguished Chair in Nanoelectronics.

Supporting Information Available: Additional information including the analysis of Si-capped $HfSe_2$ thin films, CVT-grown $HfSe_2$ crystals, and XRD data of MBE-grown $HfSe_2$ thin films can be found in the Supporting Information. This material is available free of charge *via* the Internet at http://pubs.acs.org.

REFERENCES AND NOTES

1. Mayorov, A. S.; Gorbachev, R. V.; Morozov, S. V.; Britnell, L.; Jalil, R.; Ponomarenko, L. A.; Blake, P.; Novoselov, K. S.; Watanabe, K.; Taniguchi, T. Micrometer-Scale Ballistic Transport in Encapsulated Graphene at Room Temperature. *Nano Lett.* **2011**, *11*, 2396–2399.
2. Balandin, A. A.; Ghosh, S.; Bao, W.; Calizo, I.; Teweldebrhan, D.; Miao, F.; Lau, C. N. Superior Thermal Conductivity of Single-Layer Graphene. *Nano Lett.* **2008**, *8*, 902–907.
3. Mattheiss, L. Band Structures of Transition-Metal-Dichalcogenide Layer Compounds. *Phys. Rev. B* **1973**, *8*, 3719.
4. Wang, Q. H.; Kalantar-Zadeh, K.; Kis, A.; Coleman, J. N.; Strano, M. S. Electronics and Optoelectronics of Two-Dimensional Transition Metal Dichalcogenides. *Nat. Nanotechnol.* **2012**, *7*, 699–712.
5. Jaegermann, W.; Tributsch, H. Interfacial Properties of Semiconducting Transition Metal Chalcogenides. *Prog. Surf. Sci.* **1988**, *29*, 1–167.
6. Chhowalla, M.; Shin, H. S.; Eda, G.; Li, L.-J.; Loh, K. P.; Zhang, H. The Chemistry of Two-Dimensional Layered Transition Metal Dichalcogenide Nanosheets. *Nat. Chem.* **2013**, *5*, 263–275.
7. Saiki, K.; Ueno, K.; Shimada, T.; Koma, A. Application of Van Der Waals Epitaxy to Highly Heterogeneous Systems. *J. Cryst. Growth* **1989**, *95*, 603–606.
8. Gong, C.; Zhang, H.; Wang, W.; Colombo, L.; Wallace, R. M.; Cho, K. Band Alignment of Two-Dimensional Transition Metal Dichalcogenides: Application in Tunnel Field Effect Transistors. *Appl. Phys. Lett.* **2013**, *103*, 053513.
9. Mak, K. F.; Lee, C.; Hone, J.; Shan, J.; Heinz, T. F. Atomically Thin MoS_2: A New Direct-Gap Semiconductor. *Phys. Rev. Lett.* **2010**, *105*, 136805.
10. Splendiani, A.; Sun, L.; Zhang, Y.; Li, T.; Kim, J.; Chim, C.-Y.; Galli, G.; Wang, F. Emerging Photoluminescence in Monolayer MoS_2. *Nano Lett.* **2010**, *10*, 1271–1275.

11. Li, T.; Galli, G. Electronic Properties of MoS_2 Nanoparticles. *J. Phys. Chem. C* **2007**, *111*, 16192–16196.
12. McDonnell, S.; Addou, R.; Buie, C.; Wallace, R. M.; Hinkle, C. L. Defect-Dominated Doping and Contact Resistance in MoS_2. *ACS Nano* **2014**, *8*, 2880–2888.
13. Kuc, A.; Zibouche, N.; Heine, T. Influence of Quantum Confinement on the Electronic Structure of the Transition Metal Sulfide TS_2. *Phys. Rev. B* **2011**, *83*, 245213.
14. Koma, A.; Sunouchi, K.; Miyajima, T. Fabrication and Characterization of Heterostructures with Subnanometer Thickness. *Microelectron. Eng.* **1984**, *2*, 129–136.
15. Koma, A.; Yoshimura, K. Ultrasharp Interfaces Grown with Van Der Waals Epitaxy. *Surf. Sci.* **1986**, *174*, 556–560.
16. Ohuchi, F.; Parkinson, B.; Ueno, K.; Koma, A. Van Der Waals Epitaxial Growth and Characterization of $MoSe_2$ Thin Films on SnS_2. *J. Appl. Phys.* **1990**, *68*, 2168–2175.
17. Ueno, K.; Abe, H.; Saiki, K.; Koma, A. Heteroepitaxy of Layered Semiconductor Gase on a GaAs (111) B Surface. *Jpn. J. Appl. Phys.* **1991**, *30*, L1352.
18. Ohuchi, F.; Shimada, T.; Parkinson, B.; Ueno, K.; Koma, A. Growth of $MoSe_2$ Thin Films with Van Der Waals Epitaxy. *J. Cryst. Growth* **1991**, *111*, 1033–1037.
19. Koma, A. Van Der Waals Epitaxy—a New Epitaxial Growth Method for a Highly Lattice-Mismatched System. *Thin Solid Films* **1992**, *216*, 72–76.
20. Ueno, K.; Saiki, K.; Shimada, T.; Koma, A. Epitaxial Growth of Transition Metal Dichalcogenides on Cleaved Faces of Mica. *J. Vac. Sci. Technol., A* **1990**, *8*, 68–72.
21. Greenaway, D. L.; Nitsche, R. Preparation and Optical Properties of Group IV−VI_2 Chalcogenides Having the CdI_2 Structure. *J. Phys. Chem. Solids* **1965**, *26*, 1445–1458.
22. Gaiser, C.; Zandt, T.; Krapf, A.; Serverin, R.; Janowitz, C.; Manzke, R. Band-Gap Engineering with Hfs_xSe_{2-x}. *Phys. Rev. B* **2004**, *69*, 075205.
23. Kreis, C.; Traving, M.; Adelung, R.; Kipp, L.; Skibowski, M. Tracing the Valence Band Maximum during Epitaxial Growth of HfS_2 on WSe_2. *Appl. Surf. Sci.* **2000**, *166*, 17–22.
24. Ōnuki, Y.; Inada, R.; Tanuma, S.-i.; Yamanaka, S.; Kamimura, H. Electrical Properties of Lithium Intercalated TiS_2, $ZrSe_2$, $HfSe_2$, 1T-TaS_2 and VSe_2. *J. Phys. Soc. Jpn.* **1982**, *51*, 880–887.
25. Zheng, X.-g.; Kuriyaki, H.; Hirakawa, K. Electrical Anisotropy of Layered Compound $ZrSe_2$ and $HfSe_2$. *J. Phys. Soc. Jpn.* **1989**, *58*, 622–626.
26. Geim, A.; Grigorieva, I. Van Der Waals Heterostructures. *Nature* **2013**, *499*, 419–425.
27. Podzorov, V.; Gershenson, M.; Kloc, C.; Zeis, R.; Bucher, E. High-Mobility Field-Effect Transistors Based on Transition Metal Dichalcogenides. *Appl. Phys. Lett.* **2004**, *84*, 3301–3303.
28. Supporting Information.
29. Li, H.; Zhang, Q.; Yap, C. C. R.; Tay, B. K.; Edwin, T. H. T.; Olivier, A.; Baillargeat, D. From Bulk to Monolayer MoS_2: Evolution of Raman Scattering. *Adv. Funct. Mater.* **2012**, *22*, 1385–1390.
30. Nathan, M.; Smith, J.; Shafer, M. In Raman Scattering from Group 4 Transition-Metal Di-Chalcogenides. *Bull. Am. Phys. Soc.* **1972**, *17*, 336.
31. Katkanant, V.; Kirby, R. D. Mixed-Crystal Lattice Dynamics of Hf_X $Ti_{1-x}Se_2$. *Phys. Rev. B* **1989**, *40*, 1152.
32. Kirihata, H.; Uda, M. Externally Quenched Air Counter for Low-Energy Electron Emission Measurements. *Rev. Sci. Instrum.* **1981**, *52*, 68–70.
33. Wagner, C.; Davis, L.; Zeller, M.; Taylor, J.; Raymond, R.; Gale, L. Empirical Atomic Sensitivity Factors for Quantitative Analysis by Electron Spectroscopy for Chemical Analysis. *Surf. Interface Anal.* **1981**, *3*, 211–225.
34. Noh, J.; Kim, H.; Kim, Y. Stability and Electronic Structures of Native Defects in Single-Layer MoS_2. *Phys. Rev. B* **2014**, *89*, 205417.
35. 2D Semiconductors, http://www.2dsemiconductors.com/category-s/1891.htm.
36. Santosh, K. C. *First-Principles Study of Novel Interfaces for Electronic Device and Energy Storage Applications*. Ph.D. Dissertation, University of Texas at Dallas, December 2014.
37. Yamamoto, H.; Yoshii, K.; Saiki, K.; Koma, A. Improved Heteroepitaxial Growth of Layered $NbSe_2$ on GaAs (111) B. *J. Vac. Sci. Technol., A* **1994**, *12*, 125–129.
38. SPI Supplies, http://www.2spi.com/.
39. Herrera-Gomez, A. *AAnalyzer*; CINVESTAV: Queretaro, MX, aherrera@qro.cinvestav.mx, 2002.
40. Herrera-Gomez, A.; Hegedus, A.; Meissner, P. Chemical Depth Profile of Ultrathin Nitrided SiO_2 Films. *Appl. Phys. Lett.* **2002**, *81*, 1014–1016.
41. Wallace, R. M. In-Situ Studies on 2D Materials. *ECS Trans.* **2014**, *64*, 109–116.
42. Horcas, I.; Fernandez, R.; Gomez-Rodriguez, J.; Colchero, J.; Gómez-Herrero, J.; Baro, A. Wsxm: A Software for Scanning Probe Microscopy and a Tool for Nanotechnology. *Rev. Sci. Instrum.* **2007**, *78*, 013705.
43. Michaelson, H. B. The Work Function of the Elements and Its Periodicity. *J. Appl. Phys.* **1977**, *48*, 4729–4733.